

FRB 20121102A monitoring: updated periodicity at L-band.

C. A. Braga^{★1,2}, M. Cruces^{3,4,5,6,2}, T. Cassanelli⁷, M.C. Espinoza-Dupouy¹, L. Rodriguez⁸, L. G. Spitler⁶, J. Vera-Casanova^{2,5}, and P. Limaye^{6,9}

¹ Departament of Astronomy, Universidad de Chile, Camino El Observatorio 1515, Las Condes, Santiago, Chile

² Centre of Astro-Engineering, Pontificia Universidad Católica de Chile, Av. Vicuña Mackenna 4860, Santiago, Chile

³ Joint ALMA Observatory, Alonso de Córdova 3107, Vitacura, Santiago, Chile

⁴ European Southern Observatory, Alonso de Córdova 3107, Vitacura, Casilla 19001, Santiago de Chile, Chile

⁵ Department of Electrical Engineering, Pontificia Universidad Católica de Chile, Av. Vicuña Mackenna 4860, Santiago, Chile

⁶ Max-Planck-Institut für Radioastronomie, Auf dem Hügel 69, D-53121 Bonn, Germany

⁷ Department of Electrical Engineering, Universidad de Chile, Av. Tupper 2007, Santiago 8370451, Chile

⁸ Instituto de Astrofísica, Facultad de Física, Pontificia Universidad Católica de Chile, Casilla 306, Santiago 22, Chile

⁹ Argelander Institute for Astronomy, 53121 Bonn

Received September XX, XXXX; accepted March XX, XXXX

ABSTRACT

Context. FRB 20121102A was the first fast radio burst to be observed to repeat. Since then, thousands of bursts have been detected by multiple radio telescopes around the world. Previous work has shown an indication of a cyclic activity level with a periodicity around 160 days. Knowing when the source repeats is essential for planning multi-wavelength monitoring to constrain their emission extent and progenitor source.

Aims. We report the monitoring of FRB 20121102A using the 100-m Effelsberg radio telescope at L-band and update the periodicity of the cyclic activity-level.

Methods. We use the Lomb-Scargle periodogram on a sample of 284 observing epochs where 42 % correspond to detections and 58 % to non-detections. Our dataset is composed of the 7 epochs of our monitoring plus publicly available data. We investigate two methods, i) binary model, describing the observing epochs with 1 if there are detections and with 0 for non-detections. ii) normalised rates model: which considers the inferred detections rates.

Results. We report no detections in 12.5-hour observations down to a fluence of 0.29 Jy ms. The best period found for the cyclic activity window is 159.3 ± 0.8 days for the binary model and 159.3 ± 0.2 days for the normalised rates model. The activity phase is shown to be 53 %. The normalised rates show a clear Gaussian-like behaviour for the activity level, where the number of detections peak at the centre of the activity window.

Conclusions. The periodicity found through both methods is consistent for the L and S-band datasets implying it is intrinsic to the source. The activity phase in S-band however shows an indication of it ending before the L-band activity phase, supporting the idea of chromatic dependence of the activity window. The sample at C-band however is not large enough to further confirm this result.

Key words. methods: observational – fast radio bursts – radio continuum: transients

1. Introduction

Fast radio bursts (FRBs) are highly energetic (10^{36} – 10^{41} erg) radio pulses with durations ranging from microseconds to milliseconds that come from extragalactic sources (Lorimer et al. 2007). They are characterised by a frequency-dependent time delay in their arrival times, which is quantified by the dispersion measure (in units of pc cm^{-3} ; DM) and corresponds to the column density of free electrons between the observer and the source. Based on their detection we can categorise them with two types: one-offs, which have been detected only once, and repeaters. Morphological studies of FRBs show that one-offs and repeaters have distinguished spectral and time structure (Pleunis et al. 2021) suggesting that they come from different populations and potentially having different origins. From the repeaters only two sources exhibit periodic activity windows: FRB 20180916B (CHIME/FRB Collaboration et al. 2020) with a periodicity of 16.35 days and FRB 20121102A with a periodicity of 157 days found in Rajwade et al. (2020) and 161.3 days found later in

Cruces et al. (2021b). FRB 20180916B has an active window (the phase where the bursts are detected) of ~ 31 % which means that for 5 days out of the 16 (CHIME/FRB Collaboration et al. 2020) the source is active. For FRB 20121102A the activity window is ~ 60 %, which means that out of the 161 days the source is active for roughly 97 days (Cruces et al. 2021b). The first repeater ever detected, FRB 20121102A, (Spitler et al. 2016) was localised by Very Long Baseline Interferometric observations to its host, a low-metallicity, star-forming dwarf galaxy at redshift $z = 0.19273(8)$ (Chatterjee et al. 2017; Tendulkar et al. 2017). One of the explanations for the periodic behavior of FRBs is a formation scenario involving a binary system, where the periodicity arises from the orbital period. Another possibility, pointed out for FRB 20180916B is that the periodicity is due to the precession of a magnetar (Feng et al. 2024). Even though we still do not know the origin of these FRBs, their periodic behaviour makes follow-up observations and multi-wavelength campaigns easier, allowing us to characterise their emission extent and therefore constrain their progenitor source.

★ Email: cristobal.braga@ug.uchile.cl

Table 1. FRB 20121102A monitoring setup with Effelsberg.

Start date (UTC)	Duration (s)	Sample time (μ s)	Number of channels
2022-09-18 10:08:48	7188	51.2	512
2022-09-18 23:58:13	8983	51.2	512
2022-11-19 23:10:17	4753	51.2	1024
2023-02-25 18:53:49	1276	51.2	512
2023-06-29 14:54:23	5390	25.6	512
2023-08-19 03:10:42	10650	25.6	512
2023-11-17 01:41:03	7107	25.6	512

Notes. Start time of the FRB 20121102A observations taken with the 100-m Effelsberg radio telescope in UTC, their duration in seconds, sample time and number of frequency channels. All observations have the same central frequency at 1400 MHz and bandwidth of 400 MHz.

In this paper, we report the follow-up observations of FRB 20121102A at L-band using the 100-m Effelsberg radio telescope and the updated periodicity results. In Sect. 2, we describe the setup of our observations. In Sect. 3, we present the techniques used to combine our dataset with all publicly available observations of the source. In Sect. 4, we present the results of the follow-up and the updated periodicity and activity window. In Sect. 5, we discuss the implications of periodicity for FRB 20121102A, and in Sect. 6, we present our final remarks and conclusions.

2. Follow-up

The dataset consisted of 12.5 h of observations of FRB 20121102A taken in September 2022, February 2023, June 2023, August 2023, and November 2023. These observations were not scheduled based on the activity of the source but instead carried out as blind observations when the telescope was available. The data was taken with the Effelsberg 100-m telescope located in Germany. The observation details are presented in Table 1. The telescope has a system equivalent flux density (SEFD) of 17 Jy and a minimum fluence threshold of 0.15 Jy ms considering bursts with a 1 ms duration, a 300 MHz bandwidth and a minimum signal-to-noise ratio (S/N) of 7 (Cruces et al. 2021b). The telescope was pointed at RA: 05:31:58.600 and Dec: +33:08:49.600 to look for FRB 20121102A events. At the start of each scheduling block we started with a short 2–3 minutes observation on the bright pulsar PSR B0355+54 (pointing to RA: 03:58:53.7000 and Dec: 54:13:13.8000). This observation was conducted to verify that the system setup and conditions for observing FRB 20121102A were optimal.

The observations were carried out with the central beam of the 7-beam receiver (a description of this can be found in Cruces et al. 2021a) in combination with Effelsberg’s direct digitalisation system (EDD) with a 400 MHz bandwidth at central frequency of 1400 MHz with several time and frequency resolutions, going from 51.2 μ s and 512 frequency channels, to 25.6 μ s and 1024 frequency channels in the largest dataset.

3. Data processing

The data were in PSRFITS (Hotan et al. 2004) format with 4 Stokes parameters and were converted to intensity filterbanks using the `digifil` routine from `dspsr` (van Straten & Bailes 2011). Once converted the files were processed using a custom PRESTO-based (Ransom 2011) pipeline implemented in Python. The pipeline was tested using data collected in each observing epoch from the test pulsar, PSR B0355+54. For each epoch single pulses from this source were found down to a

S/N of 7, showing that the pipeline was working correctly. The pipeline executes the radio frequency interference (RFI) mitigation routine `rfifind` to generate a mask file to later be used in the next stages of processing. The data of FRB 20121102A were incoherently dedispersed (Lorimer & Kramer 2004) using a DM range from 550–570 pc cm⁻³ with a step of 1 pc cm⁻³ and a downsampling factor of 8 was applied to the timeseries. We searched for candidates down to a minimum S/N of 7. The timeseries for the different DM trials were used to finally run the single pulse search. After obtaining the pulse candidates we removed duplicates by clustering events whose arrival time is within a window defined by the dispersive delay of the DM trials and kept the ones with the highest S/N. The final candidates were plotted with a custom made waterfall plot and visually inspected to determine whether they were real events, RFI or other artefacts.

4. Results

4.1. Non-detections

No bursts were detected in 12.5 h of data of FRB 20121102A at L-band frequencies taken with Effelsberg down to a S/N of 7. This means, no detections down to a fluence¹ of 0.29 Jy ms considering the average of the pulse width² from the bursts reported in Cruces et al. (2021b). This fluence corresponds to an isotropic energy of 1.31×10^{38} erg.

4.2. Periodicity

The observations detailed in Table 1 were added to a dataset containing several observation dates gathered from the literature. As there is evidence of chromaticity in the start and duration of the active windows of FRB 20180916B and FRB 20121102A (Bethapudi et al. 2023; Pastor-Marazuela et al. 2021), we separated the datasets of observations into L, S, and C-bands, where L-band covers frequencies from 1 GHz to just below 2 GHz, S-band spans from 2 GHz to just below 4 GHz, and C-band ranges from 4 GHz to just below 8 GHz.

4.2.1. L-band dataset

The dataset is made from the observations reported in Spitler et al. (2014); Scholz et al. (2016); Spitler et al. (2016); Scholz et al. (2017); Hardy et al. (2017); Marcote et al. (2017); Houben et al. (2019); Oostrum et al. (2020); Rajwade et al. (2020); Caleb et al. (2020); Li et al. (2021); Cruces et al. (2021b); Hewitt et al. (2022); Jahns et al. (2023); Feng et al. (2023); Zhang et al. (2024) and the observations reported in this work. The dataset contains observations made with Effelsberg, the Arecibo Observatory with the Arecibo L-Band Feed Array (ALFA) and L-wide receivers, the Westerbork Synthesis Radio Telescope (WSRT), the Five-hundred-meter Aperture Spherical radio Telescope (FAST), the Green Bank Telescope (GBT), the Lovell Telescope (LT), the Meerkat Telescope, the Very Large Array (VLA) and the Deep Space Network telescopes 43 and 63 (DSS-43 and DSS-63). We made sure to only include each observation once, as some were reported more than once by different authors. The timestamps used correspond to the modified Julian date (MJD) marking the start of each observation. In case of only

¹ In this work we compute fluence based on the band-averaged peak flux density.

² We refer to the band-averaged pulse width as pulse width.

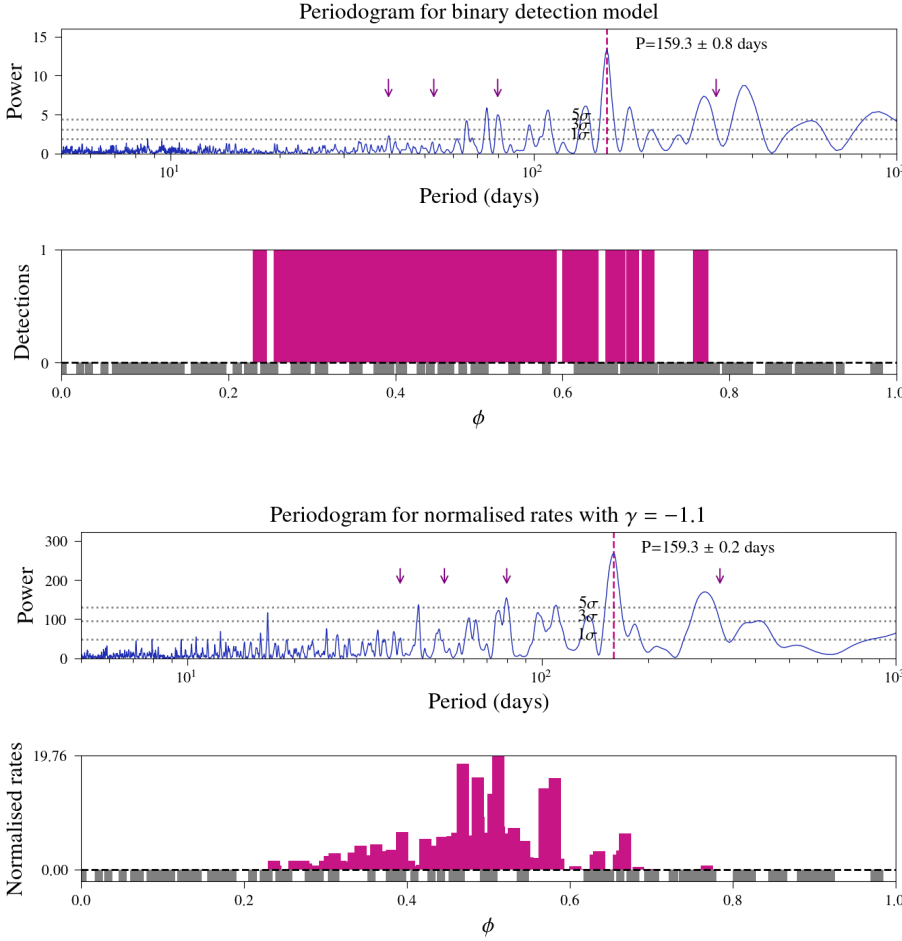


Fig. 1. *Top:* L-band dataset periodogram resulting from the binary model with detection labels (0 for non-detections and 1 for detections). The first candidate of the periodogram yields a periodicity of 159.3 ± 0.8 days. The arrows indicate some of the harmonics of the period found. Two peaks to the right around 290 and 380 days are as well prominent. The dotted horizontal lines correspond to the 1σ , 3σ and 5σ significance levels determined by 10 000 bootstrap resamplings. *Bottom:* Folding of the observations with a periodicity of 159.3 days. MJD 58 356.5 is used as reference epoch with phase $\phi = 0$. In magenta the detections are labelled with 1 and in grey the non-detections are labelled with 0 (a little height was added to these so they are visible in the plot).

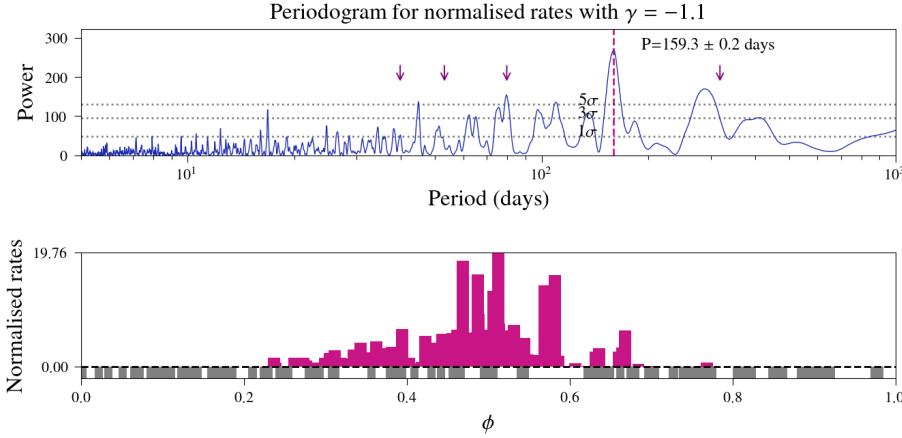


Fig. 2. *Top:* L-band dataset periodogram for the normalised rates model. The arrows indicate some of the harmonics of the 159 days period. The peaks to the right of the plot are roughly at 290 and 380 days. They arise due to the superposition of the spacing of the two most active epochs of FRB 20121102 plus the 2nd harmonic of the 159 days. The dotted horizontal lines correspond to the 1σ , 3σ and 5σ significance levels determined by 10 000 bootstrap resamplings. *Bottom:* Observations folding at 159 days. In magenta are highlighted observations with detections and in grey the non-detections. A small height was added to the non-detections for visualisation of phase domain coverage. The activity phase, described by the magenta bars shows a Gaussian-like profile, where the detections peak in the centre.

reported MJDs of detected bursts we used the MJDs of the bursts and the wait times between them to determine approximate start of observation times. We included in the dataset a single burst reported in Feng et al. (2023) because there is a lack of detections between 2021 and 2023. The full dataset consists of 284 epochs in a total time span of 4031 days with 165 non-detections and 119 detections. We use the Lomb-Scargle periodogram (VanderPlas 2018) technique to find the periodicity of the source and find a periodicity of 159.3 ± 0.8 days which is in very good agreement with the 161.3 ± 5.0 days found in Cruces et al. (2021b).

We try two different methods to model the detections in order to calculate the periodicity. We use a “binary model” and a “normalised rate model”. In the first one detections are labelled with 1 and no detections are labelled with 0 similarly as in Cruces et al. (2021b). We obtained a periodicity of 159.3 ± 0.8 days for the binary model. We estimate the false alarm probability of the peak by using a bootstrap resampling with 10 000 trials. We get a peak significance above 5σ and smaller uncertainty than Cruces et al. (2021b). Figure 1 shows the result of the periodogram.

The $1\sigma_{LS}$ uncertainty for the period is calculated using the full width half maximum (FWHM) of the Gaussian fit to the peak as formulated by VanderPlas (2018):

$$\sigma_{LS} = \frac{FWHM}{2} \sqrt{\frac{2}{N \times (S/N)^2}} \quad (1)$$

where N is the number of points in the dataset.

Along with the binary detection model, we used a more sophisticated model in which we instead use the rates of detections,

calculated as the number of detected bursts within the observation length for each observation in our dataset. To address the difference in sensitivity across the telescopes, we translate the rates to what a 100-m telescope would infer. We refer to this rate as *normalised rate*, and we calculate it as:

$$R_{\text{norm}} = R_{\text{ref}} \left(\frac{F_{\text{min}}}{F_{\text{ref}}} \right)^\gamma, \quad (2)$$

where R_{ref} is a reference rate obtained from an observation, F_{min} is the minimum detectable fluence of the telescope we use to normalise, F_{ref} is the minimum detectable fluence of the telescope from which we take the reference rate at a given observing frequency and γ is the power-law value that describes the cumulative energy distribution of the bursts for a given FRB. We consider a gamma value of -1.1 as reported in Cruces et al. (2021b). The fluence of a pulse is given by (radiometer equation):

$$F = \frac{S/N \times \text{SEFD}}{\sqrt{n_p \times \Delta\nu}} \times \sqrt{\Delta t} \quad (3)$$

where the S/N is taken to be 7, n_p is the number of polarisations taken to be 2, Δt is the pulse width considered to be 1 ms, and $\Delta\nu$ is the observation bandwidth. One bias in this model is that, although the detections are weighted relative to each other by the event rate, all non-detections are weighted equally, regardless of their duration. To mitigate this, we have split the non-detections into 1-hour blocks (each representing 0 events/hour). We removed the blocks of non-detections that were left with a duration of less than 1-hour after the split. We consider the bias

in this approach less significant than treating each non-detection observation as an independent data point, regardless of its duration.

The periodogram for this dataset yields a periodicity of 159.3 ± 0.2 days, which is consistent with the one obtained from the binary model. As shown in Fig. 2, the significance of this peak is greater than 5σ but lower than the one from the binary model. This is expected because, in comparison with the binary model, the same number of observations are now split into more bins, given the continuous value an inferred rate can have. Other significant peaks to the left of the 159.3 days period correspond to harmonics and the two most prominent peaks to the right of 159.3 days are a result of the time difference between the two most active reported windows for FRB 20121102A which are visible at Fig. 3.

4.2.2. S-band dataset

The same process described previously was done for a dataset of observations made in S-band. The observations were taken from Scholz et al. (2016); Law et al. (2017); Scholz et al. (2017); Majid et al. (2020); Pearlman et al. (2020); Cruces et al. (2021b). This dataset is composed of 80 epochs with 64 non-detections and 16 detections for a total time span of 1549 days. The periodicity for this dataset is 159.8 ± 1.4 days for the binary model and 163.1 ± 1.5 days for the normalised rates model, in agreement with the previous two obtained in the L-band dataset. The binary model periodogram for this dataset is shown in Fig. 4 and the normalised rate model periodogram in Fig. 5.

4.2.3. C-band dataset

The dataset of observations from C-band were taken from Scholz et al. (2016); Law et al. (2017); Spitler et al. (2018); Michilli et al. (2018); Gajjar et al. (2018); Cruces et al. (2021b). This dataset is comprised of 49 epochs with 43 non-detections and 6 detections for a total time span of 673 days. We find no periodicity for this dataset. This is likely due to the low number of detections present in the data.

5. Discussion

The results obtained for the periodicity of FRB 20121102A are consistent and further improve the previously reported in Cruces et al. (2021b) because our dataset contains more epochs and an extended time span. We tried the method of normalising the rates to test whether it improves the estimation of the periodicity of FRB 20121102A and find a period of 159.3 ± 0.2 days. The advantage of the normalised rate model is that it weighs each timestamp by the level of activity within it. In comparison with the 159.3 ± 0.8 days obtained from the binary model, both peaks have a significance greater than 5σ but the normalised rate model has a lower significance than the binary model. We attribute the difference to the fact that in the binary model the power of the signal is split between detections (1) and non-detections (0), while in the normalised rate model the power is distributed in a wider bin range. This introduces as well more noise to the time-series. An in-depth analysis of the different methods to estimate the periodicity is work in progress.

Additionally, a more accurate model for the normalised rates would consider different γ values in eq. (2) for each telescope in the dataset. To test the importance of the parameter in our results, aside from the $\gamma = -1.1$ obtained in Cruces et al. (2021b) we try

using $\gamma = -1.37$ reported in Li et al. (2021) and obtain a consistent periodicity. Therefore because we used Effelsberg as our reference in the normalisation we consider that using $\gamma = -1.1$ for all telescopes is optimal. Because of the higher significance of the peak in the binary model, we take this as the new best periodicity for FRB 20121102A. To centre the activity window around a phase of $\phi = 0.5$, we use the MJD 58356.5 as a reference epoch for phase $\phi = 0$ and we get an activity window of 53 %. This means, that roughly out of the 159 days duration of one cycle, the source is active within a 84 days window at L-band. This is broader than the 31% for FRB 20180916B (CHIME/FRB Collaboration et al. 2020).

As it is seen in Fig. 2 the highest peak in the periodogram of the normalised rates is 159 days, followed in second place by the peak at 290 days. A third peak around 380 days is also significant. As marked in the periodogram with the purple arrows, the peak at 290 days superposes with the 2nd harmonic of the 159 days peak. These peaks are also seen in the periodogram of the binary model but with significantly lower power. By plotting all the observing epochs against their normalised rate as shown in Fig. 3 we observe that the two most active windows correspond to 2018 with the observations of Arecibo from the “November rain” (Jahns et al. 2023) and to 2019 with the FAST telescope observations (Li et al. 2021). This introduces an artefact in the calculation of the periodicity. The peaks at 290 and 380 days can be explained by the spacing between these high-activity episodes, with intervals ranging from 270 days for the closest observations to 370 days for the furthest apart. To verify that such peaks correspond to artefacts, we fold the epochs using the above mentioned reference epoch. The result from folding at 290 and 380 days is the distribution of epochs with detections all over the phase space, with no clear trend. We only find a dispersion optimised distribution of the detection epochs for the 159 days period. This is shown at the bottom of the periodogram in Fig. 2. Observations triggered by known activity of the source may introduce bias in the calculation of the periodicity. In our case, since we have 58 % non-detections and 42 % detections this bias is minimised.

From the folding it is clearly seen that the active phase has a Gaussian-like profile, where the peak of the detections are located in the middle of the window. This behaviour has as well been seen for FRB 20180916B (CHIME/FRB Collaboration et al. 2020). Overall, we conclude that although the normalised rate model has greater physical meaning, more data is needed to achieve the same or higher level of significance than the binary model.

Regarding the dependence of the activity window with the observing frequency, we obtain for the L and S-band a consistent period. For the normalised rate model the 163.1 days value obtained for the periodicity is consistent with both the S-band binary model and with the L-band value within 2.5σ . This means that the phenomena leading to the active phase of the source is intrinsic. However, as is seen in the folding of the S-band dataset shown in Fig. 4, the full phase range is not mapped. In particular we lack observations in a considerable part of the phase, towards the start of the activity. We do not see a clear gaussian-like trend as it is appreciated in the L-band dataset, probably because of the limited dataset. More observations in this band will permit a quantitative comparison across frequencies.

Folding the S-band dataset with the periodicity obtained at L-band we find that the activity window for S-band ends before the L-band activity window, having a phase difference of 0.12. This means that the S-band activity phase finishes 19 days before the L-band active phase. Since we do not have the 0–0.4 part of

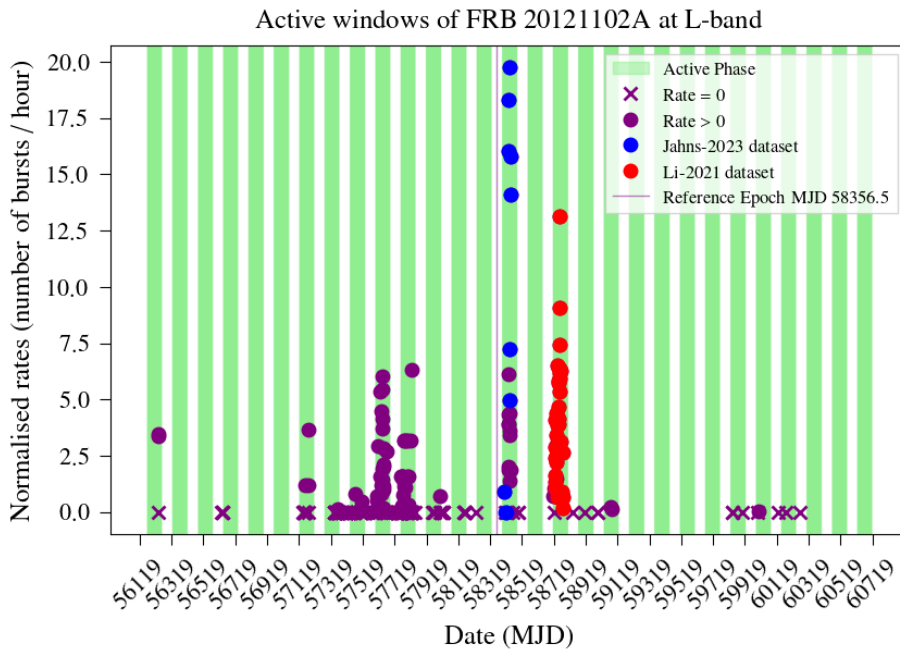


Fig. 3. Normalised rates vs MJD spanning from the oldest window where FRB 20121102A has been observed at L-band to the current active window. The active phase of FRB 20121102A displayed with the green bands correspond to a 53 % of the phase and a period of 159.3 ± 0.8 . The reference epoch is MJD 58 356.5 for phase of 0. In blue and red are highlighted the observations from November rain (Jahns et al. 2023) and FAST’s sample (Li et al. 2021), respectively.

the phase completely mapped in S-band we cannot conclude for certain what happens in this part.

Regarding the C-band dataset, we do not have enough observations and in particular detections for the Lomb-Scargle periodogram to output a consistent periodicity. More observations will help better understand the shift in phase between frequency bands and the behaviour of the activity phase (Espinoza-Dupouy et al. in prep.).

Using our 159.3 days periodicity, 53% of active phase and our reference epoch of 58 356.5 we calculate that as of August 2024 the source is at 0.6 phase and the next active phase should begin on 2024-11-12 UTC and end in 2025-02-03 UTC. We emphasise that this does not guarantee detections of the source, but rather indicates when the source is most likely to emit.

Our result for the periodicity is consistent with the recent work of Li et al. (2024). Unlike their approach, which considers the MJDs of the bursts independently of the frequency band, we separated the observing epochs based on the frequency at which the observations were conducted. They report a candidate period of $157.1^{+5.2}_{-4.8}$ and another of $4.605^{+0.003}_{-0.010}$ days using a phase-folding algorithm. The second candidate period was not detected in their Lomb-Scargle periodogram, nor does it appear in ours. Furthermore, we folded the dataset at the trial period and no trend was seen. Given the chromatic behaviour observed in the active windows of FRB 20180916B (Bethapudi et al. 2023) and hint for dependence in FRB 20121102A presented in our work, we believe a frequency separation to be necessary. Naturally, more observations across the frequency range will help pinpoint the magnitude of the shift and the duration of the activity window.

The widely accepted scenarios to explain periodic actively repeating FRBs involve either a precessing magnetar or a neutron star (NS) in a binary system. In the literature, several precession models of young, hot, non-superconducting, and highly active long-period isolated magnetars can explain the periodicity of FRB 20180916B (Beniamini et al. 2020; Feng et al. 2024). However, most of these models do not consider vortex superfluidity, which can dampen long-period precession (Shaham 1977). Therefore making this explanation for the periodicity of FRB 20121102A unlikely. Although there have been at-

tempts to reconcile long-period precession with quantum vortices, this seems to occur only under very specific conditions such as a weakly coupled toroidal magnetic field (Goglichidze & Barsukov 2019).

Alternatively, models of neutron stars in binary systems have been proposed to explain the longer timescale periodicity of FRB 20121102A (Lyutikov et al. 2020; Ioka & Zhang 2020). A neutron star with a black hole companion could induce spin precession on timescales similar to those observed in actively repeating FRBs. However, for this effect to occur, the neutron star would need to be in a close orbit around the black hole, where the typical orbital lifespan of the system is approximately 10 years. As the neutron star moves closer to the black hole, relativistic effects, such as precession and spin-up of the neutron star, should become increasingly pronounced (Yang & Zou 2020). Despite this, FRB 20121102A has been observed for over a decade and its activity windows has not shown the rate of change predicted by these models.

Another possible companion for a neutron star is a massive star that continuously emits stellar winds. As the neutron star interacts with the stellar wind of its companion, it can create activity windows that vary with frequency. To explain the observed DM of FRB 20121102A using these models, the FRB would need to be emitted when the neutron star is near the periastron of its orbit. This scenario would result in a variation of four orders of magnitude in the DM within approximately 10% of the orbital phase (Lyutikov et al. 2020). However, observations indicate that the activity window of FRB 20121102A spans about half of its cyclic period, and no DM variation of that magnitude has been observed.

6. Conclusions

We reported 7 observing epochs of FRB 20121102A monitoring and find no detections. We combined our observations with publicly available data of the source and divided it per frequency band and found a new best periodicity for the cyclic activity window to be 159.3 ± 0.8 days at L-band. This updated periodicity is more precise and with higher significance than the previously reported in Cruces et al. (2021b), mainly because of the larger

and extended dataset. We also report the same periodicity using a normalised rates model that is more precise but has less significance than the one obtained by the binary model. We found a consistent periodicity at S-band and report that this active phase seems to end 19 days before the L-band active phase. No conclusions can be drawn from the C-band observations given the lack the observing epochs and in particular of detections. We strongly encourage the community to report both detections and non-detections of repeating FRBs and the full observation details. Sky and instrumentation statistics such as exposure time, observation duration, and telescope properties are fundamental to further constrain the nature of FRBs.

Acknowledgements. This publication is based on observations with the 100-m telescope of the Max-Planck-Institut für Radioastronomie at Effelsberg. C.B. would like to thank the Max Planck Partner group at PUC led by M. C. for funding the internship that led to this work. C. B. would like to thank B. Briceño for his support and feedback during this project. T. C. acknowledges support by the ANID BASAL FB210003 and fondo de astronomía: ANID / Fondo 2023 QUIMAL/ QUIMAL230001.

References

- Beniamini, P., Wadiasingh, Z., & Metzger, B. D. 2020, *MNRAS*, 496, 3390
- Bethapudi, S., Spitler, L. G., Main, R. A., Li, D. Z., & Wharton, R. S. 2023, *MNRAS*, 524, 3303
- Caleb, M., Stappers, B. W., Abbott, T. D., et al. 2020, *MNRAS*, 496, 4565
- Chatterjee, S., Law, C. J., Wharton, R. S., et al. 2017, *Nature*, 541, 58
- CHIME/FRB Collaboration, Amiri, M., Andersen, B. C., et al. 2020, *Nature*, 582, 351
- Cruces, M., Champion, D. J., Li, D., et al. 2021a, *MNRAS*, 508, 300
- Cruces, M., Spitler, L. G., Scholz, P., et al. 2021b, *MNRAS*, 500, 448
- Feng, X.-M., Yang, Y.-P., & Li, Q.-C. 2024, *MNRAS*, 530, 3641
- Feng, Y., Jiang, J., Zhou, D., et al. 2023, *The Astronomer’s Telegram*, 15980, 1
- Gajjar, V., Siemion, A. P. V., Price, D. C., et al. 2018, *ApJ*, 863, 2
- Goglichidze, O. A. & Barsukov, D. P. 2019, *MNRAS*, 482, 3032
- Hardy, L. K., Dhillon, V. S., Spitler, L. G., et al. 2017, *MNRAS*, 472, 2800
- Hewitt, D. M., Snelders, M. P., Hessels, J. W. T., et al. 2022, *MNRAS*, 515, 3577
- Hotan, A. W., van Straten, W., & Manchester, R. N. 2004, *PASA*, 21, 302
- Houben, L. J. M., Spitler, L. G., ter Veen, S., et al. 2019, *A&A*, 623, A42
- Ioka, K. & Zhang, B. 2020, *ApJ*, 893, L26
- Jahns, J. N., Spitler, L. G., Nimmo, K., et al. 2023, *MNRAS*, 519, 666
- Law, C. J., Abuzzo, M. W., Bassa, C. G., et al. 2017, *ApJ*, 850, 76
- Li, D., Wang, P., Zhu, W. W., et al. 2021, *Nature*, 598, 267
- Li, J., Gao, Y., Li, D., & Wu, K. 2024, *ApJ*, 969, 23
- Lorimer, D. R., Bailes, M., McLaughlin, M. A., Narkevic, D. J., & Crawford, F. 2007, *Science*, 318, 777
- Lorimer, D. R. & Kramer, M. 2004, *Handbook of Pulsar Astronomy*, Vol. 4
- Lyutikov, M., Barkov, M. V., & Giannios, D. 2020, *ApJ*, 893, L39
- Majid, W. A., Pearlman, A. B., Nimmo, K., et al. 2020, *ApJ*, 897, L4
- Marcote, B., Paragi, Z., Hessels, J. W. T., et al. 2017, *ApJ*, 834, L8
- Michilli, D., Seymour, A., Hessels, J. W. T., et al. 2018, *Nature*, 553, 182
- Oostrum, L. C., Maan, Y., van Leeuwen, J., et al. 2020, *A&A*, 635, A61
- Pastor-Marazuela, I., Connor, L., van Leeuwen, J., et al. 2021, *Nature*, 596, 505
- Pearlman, A. B., Majid, W. A., Prince, T. A., et al. 2020, *ApJ*, 905, L27
- Pleunis, Z., Good, D. C., Kaspi, V. M., et al. 2021, *ApJ*, 923, 1
- Rajwade, K. M., Mickaliger, M. B., Stappers, B. W., et al. 2020, *MNRAS*, 495, 3551
- Ransom, S. 2011, *PRESTO: Pulsar Exploration and Search TOolkit*, Astrophysics Source Code Library, record ascl:1107.017
- Scholz, P., Bogdanov, S., Hessels, J. W. T., et al. 2017, *ApJ*, 846, 80
- Scholz, P., Spitler, L. G., Hessels, J. W. T., et al. 2016, *ApJ*, 833, 177
- Shaham, J. 1977, *ApJ*, 214, 251
- Spitler, L. G., Cordes, J. M., Hessels, J. W. T., et al. 2014, *ApJ*, 790, 101
- Spitler, L. G., Herrmann, W., Bower, G. C., et al. 2018, *ApJ*, 863, 150
- Spitler, L. G., Scholz, P., Hessels, J. W. T., et al. 2016, *Nature*, 531, 202
- Tendulkar, S. P., Bassa, C. G., Cordes, J. M., et al. 2017, *ApJ*, 834, L7
- van Straten, W. & Bailes, M. 2011, *PASA*, 28, 1
- VanderPlas, J. T. 2018, *ApJS*, 236, 16
- Yang, H. & Zou, Y.-C. 2020, *ApJ*, 893, L31
- Zhang, Y.-K., Li, D., Feng, Y., et al. 2024, *Science Bulletin*, 69, 1020

Table 2. Sensitivity of telescopes in the sample.

Telescope	F_{min} (Jy ms)	Frequency Band
Effelsberg	0.15	L-band
Arecibo	0.03 / 0.02	L-band (ALFA / L-Wide)
GBT	0.05	S-band
FAST	0.012	L-band
WSRT	0.26	L-band
Meerkat	0.06	L-band
DSS-43	0.23	S-band
DSS-63	0.5	S-band
VLA	0.19 / 0.06	L-band / S-band
Lovell	0.23	L-band

Notes. The first column displays the names of the radio telescopes, the second the minimum fluence values (F_{min}) for each telescope and the third column indicates the specific frequency band used.

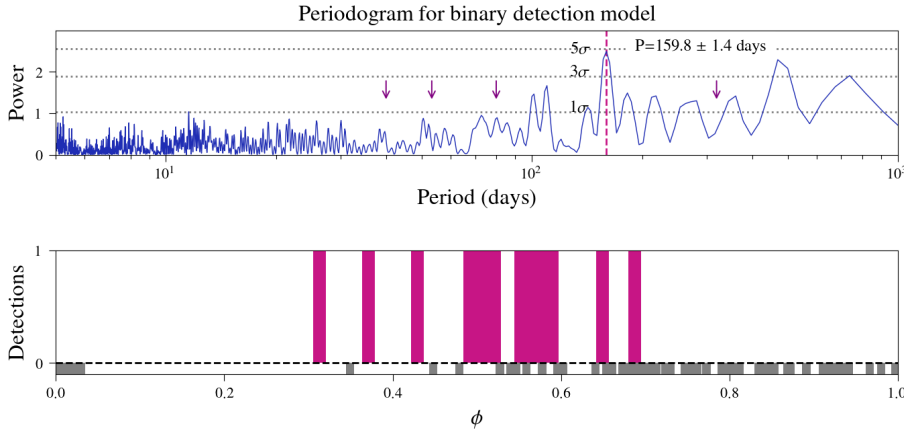


Fig. 4. *Top:* periodogram resulting from the S-band binary dataset. The periodicity this dataset yields is 159.8 ± 1.4 days. The purple arrows indicate some of the harmonics of the period found. The dotted horizontal lines correspond to the 1σ , 3σ and 5σ significance level determined by 10 000 bootstrap resamplings. The peak at 159.8 days is right below a 5σ significance. *Bottom:* Folding of the observations using the obtained periodicity. In this dataset more observations are needed to be able to map the full phase domain. In magenta are highlighted observations with detections and in grey the non-detections. A small height was added to the non-detections for visualisation of phase domain coverage.

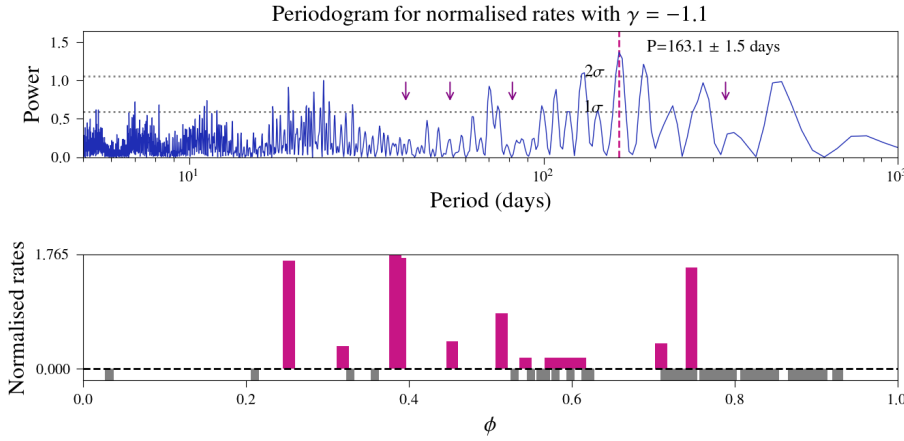


Fig. 5. *Top:* periodogram resulting from the S-band dataset with normalised rates. The periodicity of this dataset yields is 163.1 ± 1.5 days. The purple arrows indicate some of the harmonics of the period. The dotted horizontal lines correspond to the 1σ and 2σ significance level determined by 10 000 bootstrap resamplings. The peak at 163.1 days is slightly above 2σ . *Bottom:* Folded normalised rates at the obtained frequency vs phase. In magenta are highlighted observations with detections and in grey the non-detections. A small height was added to the non-detections for visualisation of phase domain coverage. No indication for a Gaussian-like activity window is present, however the phase domain is not fully sampled.